Simulating Condensational Growth, Evaporation, and Coagulation of Aerosols Using a Combined Moving and Stationary Size Grid

Mark Z. Jacobson* and Richard P. Turco
Department of Atmospheric Sciences, 405 Hilgard Ave., University of California, Los Angeles, CA 90024-1565

We present a numerical method of simulating the aerosol processes of coagulation, condensational growth, and evaporation over a hybrid size grid. In the hybrid grid, the volume of involatile core material is constant for each size bin, but the volume of volatile material fluctuates. Since particles in each bin grow and evaporate at their own pace, particles from one bin can obtain the same volume as those from another bin while maintaining different composition. Similarly, particles from different bins that grow to the same size can evaporate back to their respective original core sizes. Allowing independent growth of particles inhibits numerical diffusion since particles in each bin grow or evaporate to their actual sizes. When two particles coagulate, they form a new particle with core volume between the core volumes of particles in two other bins. We partition the new particle and its total volume between these two bins. Similarly, we adapt other processes, such as nucleation, emissions, and transport to the hybrid grid structure. The condensational growth equations developed conserve mass between the gas phase and size-distributed aerosol phase. Because the equations result in sparse matrices of partial derivatives, SMVGEAR, a sparse-matrix Gear-type integrator, solves them quickly. Furthermore, the semi-implicit coagulation equations used here conserve volume exactly, are absolutely stable, and require no iteration. Finally, we compared model solutions to both analytical and other integrated numerical solutions. To obtain numerical solutions, we developed and integrated equations that simulate simultaneous coagulation and growth of multicomponent particles.

I. INTRODUCTION

Atmospheric models often simulate aerosol processes such as nucleation, coagulation, condensational and dissolutional growth, chemical equilibrium, aqueous chemistry, and transport. Currently, several numerical schemes are available to treat condensational growth and evaporation. Among these are discrete size bin (sectional) methods (e.g., Turco et al., 1979a, b; Gelbard and Seinfeld, 1980; Seigneur, 1982; Warren and Seinfeld, 1985; Pilinis et al., 1987a; Toon et al., 1988; Rao and McMurry, 1989), finite element methods (Varoglu and Finn, 1980; Tsang and Brock, 1983, 1986; Tsang and Huang, 1990), modified upwind difference methods (e.g., Smolarkiewicz, 1983; Tsang and Korgaonkar, 1987; Kim and Seinfeld, 1990a), moments methods (e.g., Friedlander, 1983; Whitby, 1985; Lee, 1985; Brock et al., 1986; Brock and Oates, 1987), the cubic spline method (e.g., Middleton and Brock, 1976), and moving (or variable) bin methods (e.g., Mordy, 1959; Neiburger and Chien, 1960; Gelbard, 1990; Kim and Seinfeld, 1990b).

We define a stationary size bin as one where the volume of each particle in the bin is constant and the same as the vol-

*Corresponding author. Currently at Department of Civil Engineering, Ternan Engineering Center, M-13, Stanford University, Stanford, CA 94305-4020.

Aerosol Science and Technology 22:73-92 (1995)

0278-6826/95/$9.50
SSDI 0278-6826(94)00034-Y

ume of each other particle in the bin. When a particle grows (or evaporates), it transfers from its current bin to a bin containing larger (or smaller) particles. A moving bin, on the other hand, is one where the volume of each particle in the bin changes, and changes at the same rate as the volume of each other particle in the bin. Thus, when a particle grows (or evaporates), it stays in its current bin but increases (or decreases) in volume.

Every growth scheme has advantages and disadvantages associated with it. A disadvantage of many schemes is numerical diffusion, which lowers peak concentrations and spreads the distribution over a wider size interval. Numerical diffusion occurs in stationary bin models because, when mass moves to a larger or smaller bin, it often distributes itself uniformly throughout the bin. As a result, the distributed mass can quickly grow or evaporate to the next highest or lowest bin the very next time step. For a comparison of the levels of numerical diffusion in different growth models, refer to Tsang and Rao (1988).

Another problem is numerical dispersion, which appears as waves ahead of or behind the regions of high concentration. Typically, finite element methods without "upwinding" create dispersion, while those with "upwinding" eliminate dispersion but create diffusion (Tsang and Brock, 1983).

A third problem is the tracking of involatile material in multicomponent particles after growth. For example, when particles grow to a narrow distribution (e.g., in a fog) in a stationary bin model, the core material agglomerates into a few bins. Subsequently, when the particles evaporate, the aggregated materials cannot redistribute back to their original sizes unless additional information is stored.

A fourth obstacle is conserving mass of both gas and aerosols during growth. Often, growth models subtract off the amount of gas removed by aerosol growth. However, subtracting can result in negative gas concentrations, requiring subsequent adjustments. Thus, solving for the gas and aerosol concentrations together improves solutions to the growth equations.

For this paper, we used a moving size grid for growth and evaporation to overcome the problems stated above but maintained a stationary grid structure for other processes. We also derived and solved growth equations that conserve mass when it transfers from a gas to size-distributed aerosols. Among the first to use the moving bin method, Mordy (1959) and Neiburger and Chien (1960) calculated condensational growth of cloud droplets. Recently, Gelbard (1990) also discussed a moving bin growth model that Kim and Seinfeld (1990b) expanded for multicomponent aerosols. Advantages of the moving bin method are that it avoids both numerical diffusion and dispersion (Gelbard, 1990; Kim and Seinfeld, 1990b).

For other processes, such as coagulation, emissions, and nucleation, we maintained the characteristics of a stationary grid. In the case of coagulation, we modified the equations described in Jacobson et al. (1994a) for the hybrid size grid. Jacobson et al. expanded upon the semi-implicit method of Turco et al. (1979a, b) and Toon et al. (1988) to permit coagulation over any size grid and among any number of particle types, each with a different size distribution and composition.

While several models have treated single-component coagulation and condensation together (e.g., Middleton and Brock, 1976; Gelbard and Seinfeld, 1978; Warren and Seinfeld, 1985; Tsang and Hippe, 1988; Wu and Flagan, 1988), fewer have treated multicomponent coagulation and condensation simultaneously (e.g., Bassett et al., 1981; Toon et al., 1988; Kim and Seinfeld, 1990a; among others). The model developed here combines moving bin growth with stationary bin coagula-

tion for multicomponent and/or multitype aerosols.

The next section discusses growth, coagulation, and other processes using different size bin structures, and Section III describes the condensational growth equations we use. Finally, Section IV compares results to analytical and numerical solutions and Section V shows applications of the model.

II. COMPARISON OF SIZE BIN STRUCTURES

When simulating multicomponent aerosols, we can use one of several size bin structures. In this section, we compare advantages and disadvantages of just three—a completely stationary grid, a hybrid stationary-moving grid, and a completely moving grid structure.

For all cases, we assume one multicomponent particle type and define the sum of the volumes of involatile material (e.g., elemental carbon, dust, and involatile organic carbon) in a particle as the *core volume* of the particle. Non-core material can either condense onto, equilibrate with, or react with core surfaces and can dissolve into water after water condenses. We define all secondary liquids, solids, and ions that accumulate onto cores as *volatiles*, and define the *total volume* of a particle as the volume of core plus volatile material in the particle.

In all three particle grid structures, we start with any number of distinct size bins covering any range of diameters. Also, each bin contains any number of particles, and the number of particles, summed over all bins, equals the total number of particles in the system at a given time. Particle number in each bin can increase through nucleation, emissions, and transport and can decrease through deposition, sedimentation, and transport. Also, particles can change in size through condensational growth, dissolutional growth, and evaporation. Finally, while coagulation reduces total particle number, it moves particles to large sizes. Below, we discuss the differences between the three grid structures and how we treat physical processes in each.

A. Full Stationary Grid

In a stationary grid structure, particles size bins are initialized in order of increasing total (core plus volatile) volume. For example, we can initialize size bins with a geometric distribution, where the total volume of particles in one size bin equals the total volume of particles in the previous size bin multiplied by a constant (V_{RAT}). Thus, if we set $V_{RAT} = 2$, then each particle in size bin B has twice the total volume of each particle in size bin A and each particle in bin C has twice the volume of each particle in bin B, etc.

Further, in the full stationary structure, each particle in a given bin at a given time has the same total volume as each other particle in the bin, and that volume is the constant, characteristic volume of particles in the size bin. However, while each bin contains any number of particles, the number changes in time as a result of various physical processes. For example, suppose we initialize a bin structure with $V_{RAT} = 2$ and the volume of particles in the smallest bin (A) equal to 1 (generic units). Then, the volumes of particles in bins B, C, D, and E equal 2, 4, 8, and 16, respectively. Each bin contains any number of particles. Now, suppose one particle from bin B coagulates with one particle from bin C. The volume of the one resulting particle is 6, which is not represented exactly by either particle bin A, B, C, D, or E. Thus, to conserve particle number and volume, we partition half of the one new particle to bin C (volume of 4) and half to bin D (volume of 8). Consequently, coagulation reduces the number of particles in bin B by one, in bin C by

one-half, and increases the number of particles in bin D by one-half. Further, coagulation conserves volume of the coagulated particles. However, each particle in bins A, B, C, D, and E still has its initial total volume (core plus volatile volume). Thus, the primary characteristic of a stationary grid is that particles in a given bin always have a constant, characteristic total volume; however, particles can move to larger or smaller bins.

Similarly, when growth (or evaporation) occurs over a stationary grid structure, individual particles move from one size bin to a larger (or smaller) size bin. For example, if a particle of total volume 2 (bin B) grows to volume 6, then one particle is removed from bin B, one-half particle is added to bin C (volume 4), and one-half particle is added to bin D (volume 8). Thus, again, the characteristic total volume of each particle in each bin remains constant, but the number of particles in each bin changes.

Further, when emission or homogeneous nucleation occurs, certain bins gain additional particles; however, the volume of a particle in a given bin does not change. When transport occurs, particles move to nearby grid cells and replace particles that have the same total volume; thus, particles are removed from a given size bin in one spatial grid cell and added to the same size bin in an adjacent grid cell.

A second characteristic of a stationary grid relates to how components are mixed within the particles. While the total volume of a particle in a bin is constant, the core volume can range from zero to the total volume. Similarly, while the total volume of a particle in bin C is greater than the total volume of a particle in bin B by a factor of V_{RAT}, the core volume of a particle in bin C may be either greater than, equal to, or smaller than the core volume of a particle in bin B. Figure 1 illustrates how the total volumes of individual particles in three consecutive size bins (e.g., A, B, C) increase, but the core volumes are distributed without a pattern.

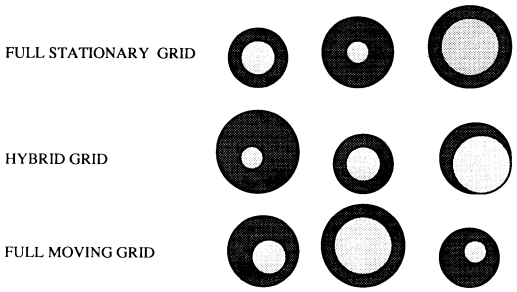

FIGURE 1. Example of sizes and compositions of representative particles in three size grid structures. For each size structure, we show three particles, each representing a different size bin. Each particle shown has two components—an involatile core and a volatile secondary component. In all structures, each size bin contains any number of particles, but all particles in a bin have the same composition and size. Thus, we represent each bin here by a single particle. In the case of the full stationary grid, the total volume (core plus volatile volume) of each particle in the first bin is smaller than the total volume of each particle in subsequent bins. However, the core volume of particles distributes randomly from one bin to the next. In the case of the hybrid grid, the core volume of each particle in the first bin is smaller than the core volume of each particle in subsequent bins. However, the total volume of particles distributes without pattern from one bin to the next. Last, in the case of the full moving grid, both core and total volumes of particles are initially ordered, but become distributed randomly from one bin to the next due to coagulation, growth, emissions, nucleation, transport, and other processes.

A stationary grid structure is most useful for simulating coagulation, nucleation, particle emission, and transport. However, it often leads to numerical diffusion during condensation and evaporation. For example, when growth occurred in the earlier example, half of a particle of volume 6 was placed in a bin with particles of volume 8, spreading the distribution arti-

ficially. Diffusion can also occur with coagulation; but, since coagulation rates are usually much slower than growth rates, diffusion is less significant with coagulation. Another problem with stationary bin growth is the loss of resolution when particles grow. For example, when aerosols activate into a fog in a stationary grid, core material from many small size bins moves into one or two large bins. By analogy, suppose all particles from bins B, C, and D grow to bin E. When particles move to bin E, volumes are averaged so that all particles in bin E have the same core and total volume. Upon evaporation, the core materials that agglomerated in bin E should evaporate back to the bins they came from. However, unless information is stored, the core materials do not "remember" whether they came from bin B, C, or D, and their redistribution becomes fairly arbitrary.

B. Hybrid Grid

A way to remedy the problems with condensational growth is to combine the stationary size bin structure with a moving bin structure in a hybrid model. In the hybrid bin structure, particle bins are initialized in order of increasing core (involatile) volume (Figure 1) as opposed to increasing total volume. For example, suppose we define $V_{\mathrm{RAT}c}$ as the volume ratio of adjacent core bins. Thus, if $V_{\mathrm{RAT}c} = 2$ and the core volume of the smallest bin (A) equals 0.1 (generic units), then the core volumes of particles in bins B, C, D, and E equal 0.2, 0.4, 0.8, and 1.6, respectively. All core bins—A, B, C, D, and E—contain any number of particles of the same average core size. Also, each particle in a given bin contains the same amount of volatile material as each other particle in the bin; but, this amount is variable. In sum, while the total volume is fixed and the core volume is variable for each particle while it resides in a given stationary size bin, the core volume is fixed and the total volume is variable for each particle while it resides in a given hybrid size bin.

When growth occurs in a stationary grid structure, particles are transferred to bins where particles have larger or smaller total volume. However, in a hybrid structure, particles are not transferred; instead, their total volumes increase or decrease to their exact sizes, eliminating numerical diffusion. For example, suppose a particle in core bin B grows from total volume 0.2 (initial core volume) to total volume of 1.3 (core plus final volatile volume). Under the stationary structure, the resulting particle would be partitioned between two size bins—one with particles of total volume smaller than and one with particles of total volume larger than 1.3. However, under the hybrid structure, particles keep their exact volume, and no particles are transferred to larger or smaller bins during growth. Thus, when the particle of total volume 1.3 evaporates, it evaporates back to its original core size of 0.2. Similarly, when a fog forms, particles in bins B, C, and D can all grow to approximately the same size, say volume 16. Upon evaporation, all particles in bins B, C, and D shrink to their original sizes of 0.2, 0.4, and 0.8. Thus, the hybrid grid eliminates two problems associated with the stationary structure—numerical diffusion and loss of information upon evaporation.

When coagulation occurs in a stationary structure, two particles collide to form a new particle. The new particle and its total volume are partitioned between two bins—one with particles of total volume smaller than and one with particles of total volume larger than the total volume of the new particle. When coagulation occurs in a hybrid structure, two particles also collide to form a third particle. However, in this case, we partition the new particle and its total volume between two

different bins—one with particles of core volume smaller than and one with particles of core volume larger than the core volume of the new particle. Thus, the main difference between coagulating in the stationary and fixed structures is how we treat the resulting particle. In reality, this new particle has unique shape and size different from those of all other particles in the atmosphere. However, with limited computer resources, we need to fit the new particle into an imperfect model size structure.

When emission of involatile material occurs in the hybrid grid, we assume the new particles enter the bin containing particles with core volume the same as the core volume of the new particles. Thus, the composition of new particles is an average composition of new and existing particles of the same core size.

When emission or homogeneous nucleation of volatile material occurs, we assume the new particles enter the bin containing particles with core volume that is the same as the total volume of the new volatile particles. By definition, these volatile particles have zero core volume. Because we mix particles containing core material with those without core material in such cases, the average core volume in a size bin decreases below the characteristic (initial) core volume of the bin. However, it never increases above the characteristic core volume. To simulate coagulation under these conditions, we assume that, when two particles combine, they form a third particle of characteristic core volume that falls between the characteristic core volume of two adjacent particles.

When transport occurs in the hybrid grid, and no volatile emissions occur, we assume particles move and replace other particles with the same core volume. Thus, the final core volume in each size bin and grid cell after transport is always the same as the initial core volume. When volatile emissions or nucleation accompany transport, we assume particles move and replace other particles with the same initial core volume.

C. Full Moving Grid

Finally, in a completely moving bin model, particles in each bin can have any core and total volume, and both the core and total volumes of particles in the bin can change during the simulation (Figure 1). For example, we can initialize bins A, B, C, D, and E with any core and volatile volume. Each bin contains any number of particles, and each particle in a bin has the same size and composition as each other particle in the same bin. Over time, however, both core and volatile volumes of each bin can change.

To treat coagulation over the full moving grid, we first rearrange particle bins from smallest to largest total volume each time step. When two particles coagulate, we partition the new particle and its total volume between two size bins—one with particles smaller than and one with particles larger than the volume of the new particle. Growth in a full moving grid occurs in the same manner as in a hybrid grid.

However, a full moving bin structure causes problems with respect to emissions, nucleation, and transport. For example, if most moving bins grow to become fog-sized drops, then few bins remain to put newly emitted particles into. In the hybrid bin case, the new particles are placed into bins that have the same core volumes as those of the emitted particles, and in the stationary bin case, the new particles are placed into bins that have the same total volumes as those of the emitted particles. Also, in the full moving bin case, when particles from all bins grow to the same total size, they have no bin to coagulate into. In a stationary

grid, particles coagulate to bins with larger total volume and in a hybrid grid, particles coagulate to bins with larger core volume.

Finally, when transport occurs in a completely moving grid, there is no way to know which particles replace which other particles in adjacent grid cells. In the hybrid case, particles of a given core volume replace others with the same core volume, and in the stationary bin case, particles of a given total volume replace others with that volume.

In sum, we use the hybrid structure because, unlike the completely stationary structure, it allows growth without numerical diffusion and allows particles to evaporate back to their original core sizes. Furthermore, unlike the completely moving structure, it permits reasonable treatment of coagulation, nucleation, emissions, and transport of particles. Next we derive growth equations and describe a method to solve them.

III. METHOD OF SOLVING GROWTH EQUATIONS

In an ideal model, we would solve the rate equations for gas-phase processes simultaneously with those for gas-aerosol transfer, inter-aerosol processes, intra-aerosol processes, and spatial transfer. While such calculations are possible on a small scale with an integrator of stiff ordinary differential equations, they currently require too much computer time for large spatial domains and aerosol size grids. A more practical approach to solving aerosol processes is to time-split (solve independently) some groups of processes while solving other groups simultaneously. With this latter approach in mind, we time-split condensational growth from coagulation and other processes.

For the most part, growth equations usually ignore the reduction in gas-phase concentrations. Here, we present and solve equations that conserve mass between the gas and aerosol phase. For the model, we assume any number of aerosol types and any number of components and size bins within each type. In the equations, N_T is the number of particle types and N_B is the number of size bins, which is the same for all types. An example of a system with three aerosol types is one which contains an elemental carbon-water type, an organic carbon-water type, and an elemental carbon-organic carbon-water type. Jacobson et al. (1994a) give a more complete description of aerosol types. In the example here, the core volume of each type consists of elemental carbon, organic carbon, and elemental plus organic carbon, respectively. The volatile material, water, can condense on all three types.

For multitype particles and a hybrid (or moving) size structure, we write the volume rate of growth or evaporation of a volatile component over a single particle as

$$\frac{d\nu_{VNi}}{dt} = (48\pi^2)^{1/3} A v_m D_{VNi}^{\text{eff}} \nu_{Ni}^{1/3} \times \left(G_V - P_V^0 B_{VNi}\right), \quad (1)$$

where ν_{VNi} is the volume (cm^3 particle^{-1}) of component V within a single particle of type N and bin i. The subscript N denotes the particle type (e.g., elemental carbon-water, organic carbon-water, or the mixture) and the subscript VN denotes each volatile component (e.g., water) of each particle type. For example each of the three particle types contains one volatile component. Thus, the Ns refer to particle types and VNs refers to individual volatile components that make up particle types.

Also, in Eq. 1, A is Avogadro's number (molecules mol^{-1}), v_m is the volume of a gas molecule (cm^3 molec^{-1}), G_V is the ambient concentration and P_V^o is the saturation vapor density (both in moles-gas

cm^{-3}-air) of gas V condensing onto particle-type N. Furthermore,

$$D_{VNi}^{\text{eff}} = \frac{D'_V \eta_{dNi} F_{vNi}}{1 + \dfrac{D'_V \eta_{dNi} F_{vNi} L_{e,V}^2 M_V^2 G_V}{K' \eta_{tNi} F_{tNi} RT^2}} \quad (2)$$

is a modified gas diffusion coefficient ($cm^2\ s^{-1}$). Factors that affect the diffusion coefficient, D'_V, are the geometry of vapor collision with small particles (e.g., Langmuir, 1944; Rooth, 1957; Mordy, 1959; Pruppacher and Klett, 1978, Toon et al., 1989) and ventilation of heat and vapor during sedimentation of large particles containing liquid (e.g., Frossling, 1938; Keith and Arons, 1954; Beard and Pruppacher, 1971; Pruppacher and Klett, 1978; Toon et al., 1989). In Eq. 2, $L_{e,V}$ is the latent heat of evaporation ($cm^2\ s^{-2}$) and M_V is the molecular weight of the condensing gas (g mol^{-1}). Also, R is the universal gas constant (erg $mol^{-1}\ K^{-1}$), T is the temperature (K), K' is the thermal conductivity of air (erg $cm^{-1}\ s^{-1}\ K^{-1}$), and F_v and F_t are ventilation factors of condensing vapor and heat, respectively (unitless). Furthermore,

$$\eta_{dNi} = \left\{1 + \left[\frac{1.33 + 0.71 Kn_{dNi}^{-1}}{1 + Kn_{dNi}^{-1}} + \frac{4(1 - \alpha_{\alpha N})}{3\alpha_{\alpha N}}\right] Kn_{dNi}\right\}^{-1} \quad (3)$$

and

$$\eta_{tNi} = \left\{1 + \left[\frac{1.33 + 0.71 Kn_{tNi}^{-1}}{1 + Kn_{tNi}^{-1}} + \frac{4(1 - \alpha_{\tau N})}{3\alpha_{\tau N}}\right] Kn_{tNi}\right\}^{-1} \quad (4)$$

are corrections to diffusivity and thermal conductivity, respectively, due to collision geometry and sticking probability (Fuchs and Sutugin, 1971; Pruppacher and Klett, 1978; Toon et al., 1989). In Eqs. 3 and 4 Kn_{dNi} and Kn_{tNi} are the Knudsen numbers of the condensing vapor and of air, respectively, α_α is the sticking coefficient of the condensing vapor, and α_τ is the thermal accommodation coefficient (Pruppacher and Klett, 1978 and Toon et al., 1989).

Next, in Eq. 1,

$$B_{VNi} = \left(1 + \frac{L_{e,V} M_V Q_{\text{rad},Ni}}{4\pi r_{Ni} RT^2 K' \eta_{tNi} F_{tNi}}\right) \times \exp\left\{\frac{2\sigma_V M_V}{r_{Ni} RT \rho_V}\right\} \quad (5)$$

is a series of adjustments to the saturation vapor pressure. Surface tension (Kelvin effect), ion content (solute effect), and radiative cooling (Barkstrom, 1978; Toon et al., 1989) alter the saturation vapor pressure of a gas over a particle. For example, the Kelvin effect increases the saturation vapor pressure over small particles, the solute effect decreases it over small and medium-sized drops, and the radiative effect decreases it over large drops. Equation 5 accounts for the Kelvin effect and radiative cooling only. The solute effect can be treated either with simple parameters or with an extensive equilibrium model. In Eq. 2 σ_V is the surface tension (dyn cm^{-1}) and ρ_V is the density (g cm^{-3}) of the condensed gas. Also, $Q_{\text{rad},Ni}$ is the radiative heating rate (erg s^{-1}—*ibid.*) and r_{Ni} is the current radius (cm) of size bin i of particle-type N.

Finally, in Eq. 1

$$\nu_{Ni} = \nu_{VNi} + \nu_{ONi} \quad (6)$$

is the volume of a single particle of type N, in bin i. The volume of the particle is the volume of the condensed gas in the particle plus the volume of all other material in the particle (ν_{ONi}). We rewrite the volume of the condensed species as $\nu_{VNi} = C_{VNi}/C_{Ni}$, where C_{VNi} is the aerosol volume concentration (cm^3-aerosol cm^{-3}-air) of component V in N_i particles, and

C_{Ni} is the number concentration (No. cm^{-3}-air) of Ni particles. Similarly, the volume of all other material in one particle is $v_{ONi} = Y_{ONi}/C_{Ni}$, where Y_{ONi} is the volume concentration (cm^3-aerosol cm^{-3}-air) of all other material in Ni particles. Combining Eq. 1 with the values in Eq. 6, we write the change in the volume concentration of condensed species VN in bin i as

$$\frac{dC_{VNi}}{dt} = C_{Ni}^{2/3}(48\pi^2)^{1/3} D_{VNi}^{\text{eff}}(Y_{ONi} + C_{VNi})^{1/3} \times \frac{M_V}{\rho_V}(G_V - P_V^0 B_{VNi}). \quad (7)$$

To conserve mass between the gas and aerosol phases, we express the rate of change of gas concentration as

$$\frac{dG_V}{dt} = -\frac{\rho_V}{M_V}\sum_{N=1}^{N_T}\left\{\sum_{i=1}^{N_B}\frac{dC_{VNi}}{dt}\right\}. \quad (8)$$

Thus, the change in gas phase concentration is proportional to the negative of the sum, over all size bins and particle types, of the change in aerosol-phase concentrations.

To obtain gas and size-distributed volatile aerosol concentrations from Eqs. 7 and 8, we need to solve $N_T \times N_B + 1$ nonlinear, first-order ordinary differential equations. The equations are even more nonlinear if we express the radius in the Kelvin term as a function of condensed aerosol concentration.

An accurate way to solve the coupled equations is with an integrator of stiff ordinary differential equations. The integrator we used, SMVGEAR (Jacobson and Turco, 1994), speeds the solution to first order equations in a large grid domain because it takes advantage of the sparsity of the matrix of partial derivatives and vectorizes around the grid-cell dimension. Since the matrix of partial derivatives resulting from Eqs. 7 and 8 requires zero fill in, SMVGEAR takes relatively little time to solve the coupled sets of these equations. When solving Eqs. 7 and 8 with an integrator, we set maximum values of dC_{VNi}/dt and its corresponding partial derivative terms during evaporation to prevent negative values of C_{VNi}. The solution to Eqs. 7 and 8 is an adjusted volume concentration of each size bin and an adjusted gas concentration. Thus, particles from different bins increase or decrease in size at their own pace, as we intended with the hybrid grid structure.

IV. COMPARISONS TO ANALYTICAL AND NUMERICAL SOLUTIONS

Here, we compare model results for condensational growth, coagulation, and a combination of the two, to results from both analytical and integrated numerical solutions. Jacobson et al. (1994a) compared the coagulation mechanism to several analytical and integrated numerical solutions; thus, we focus here primarily on testing growth alone and growth coupled to coagulation.

For the first test we compared model solutions of growth, coagulation, and a combination of both to an analytical solution given by Gelbard and Seinfeld (1978). The analytical solution assumes one particle type of uniform composition, with initial number concentration written as

$$C_i^t = \frac{C_{T,0}\, dv_i}{v_0}\exp\left(\frac{-v_i}{v_0}\right), \quad (9)$$

where $C_{T,0}$ is the total number of particles in the distribution, v_i is the volume of particles in bin i, and v_0 is mean initial volume of particles. The solution further assumes both a fixed growth rate and fixed coagulation kernel. The analytical (sub-

script a) number concentration resulting from this system is

$$C_{i,a}^{t+1} = \frac{4C_{T,0}\, d\nu_i}{v_0(\tau+2)^2} \exp\left(-\frac{2\nu_i}{v_0(\tau+2)} \times \exp(-\Lambda\tau) - \Lambda\tau \right), \quad (10)$$

where $\tau = C_{T,0}\,\beta_0 t_f$ and $\Lambda = \sigma/(C_{T,0}\,\beta_0)$. In these last equations, β_0 is the coagulation kernel (cm^3 # s^{-1}), t_f is the time interval (s), and σ is a growth rate term (s^{-1}). Also, when plotting the analytical distribution over a stationary, geometric size bin structure, we assumed $d\nu_i = 2\nu_i(V_{\mathrm{RAT}} - 1)/(V_{\mathrm{RAT}} + 1)$, where $V_{\mathrm{RAT}} = \nu_{i+1}/\nu_i$ (as discussed earlier) is the volume ratio of adjacent size bins. Also, we used $\beta_0 = 8k_B T/3\eta$, where k_B is Boltzmann's constant, T is temperature (K), and η is the dynamic viscosity of air, and assumed $C_{T,0} = 10^5$, $T = 298.15$ K, $t_f =$ 21,600 s (6 h), $V_{\mathrm{RAT}} = 1.2$, and $\Lambda = 1$. For growth alone, $\beta_0 = 0$, and for coagulation alone, $\Lambda = 0$.

To obtain a model solution for comparison, we first initialized a distribution of uniformly composed, volatile particles, assuming $V_{\mathrm{RAT}} = 1.2$. We then ran three cases: one with coagulation alone, one with coagulation combined with growth, and one with growth alone. In each case, we used thirty-six 600-s time steps. For coagulation combined with growth, we time-split (solved separately) the two processes.

To compute coagulation for this test, we modified the semi-implicit method discussed in Jacobson et al. (1994a). The lack of involatile material did not impede the calculations. For example, in the case of coagulation combined with growth, we assumed that when two particles coagulated, they formed a new particle with initial volume equal to the sum of the initial volumes of the two original particles. We then partitioned all volume of the new particle between two size bins that had initial volume smaller and larger, respectively, than the initial volume of the new particle.

Since the analytical solution required a fixed growth rate, we could not test Eqs. 7 and 8 for this particular comparison. We show results from these equations later. Instead, to solve for growth over the hybrid structure, we used

$$C_{vi,m}^{t+1} = C_{vi,m}^{t} + C_{i,m}^{t}\,\sigma\nu_i\,\Delta t, \quad (11)$$

where $C_{vi,m}^{t+1}$ is the model (subscript m) particle volume concentration (cm^3 cm^{-3}) in bin i after each Δt time step, and σ is the growth term (calculated, in this instance, from the expression for Λ, above). Also, $C_{i,m}^{t}$, for the first time step of the interval (t_f), is the initial number concentration from (9). The sum of $C_{i,m}^{t}$ over all size bins for the first time step equals C_{T0}. When no coagulation occurs, both bin-resolved and total number concentrations remain unchanged during an entire interval. However, when coagulation occurs, the particle number in each bin changes. To simulate growth under these conditions, we used the value of $C_{i,m}^{t}$ in Eq. 11 from the most recent coagulation calculation. Similarly, we used the value of $C_{vi,m}^{t}$ from the most recent coagulation and growth updates and the value of ν_i from the most recent growth update. Coagulation does not change the volume of individual particles in a size bin but it does change the total volume of material in the bin.

Figure 2 compares analytical to model solutions for growth alone, coagulation alone, and coagulation combined with growth. It shows that the hybrid grid (which allows growth with moving bins) suppressed numerical diffusion during growth. Furthermore, for the value of V_{RAT} used (1.2), the coagulation equations suppressed diffusion. For larger values of V_{RAT} (lower bin resolution), numerical diffusion slightly increases during

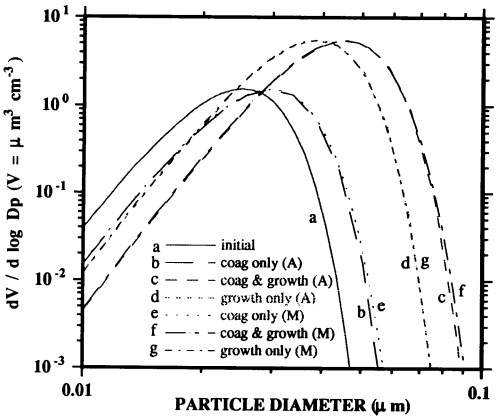

FIGURE 2. Comparison of model results (M) to analytical solutions (A) for the processes of coagulation alone, coagulation combined with growth, and growth alone. The analytical solutions (Eq. 10) are from Gelbard and Seinfeld (1978). The time interval for all solutions was 6 h, and the time step used for the model solutions was 600 s. Also, $V_{RAT} = 1.2$ for the analytical solution and for the initial model size distribution (Eq. 11). Remaining conditions are described in the text.

coagulation (Jacobson et al., 1994a). Finally, Figure 2 shows that model results for growth combined with coagulation were similar to analytical results for all sizes.

In the second test, we compared model results of coagulation combined with growth to fully-implicit integrated solutions calculated with SMVGEAR. For this example, we assumed that the size-distributed aerosol contained two components—one involatile and the other volatile. We assigned both components a hypothetical molecular weight of 150 g mol^{-1} and an aerosol-phase density of 1.5 g cm^{-3}. Further, we started with 10^6 particles cm^{-3} and distributed the particles and volume components lognormally using a geometric mean number diameter of 0.02 μm and geometric standard deviation of 1.4. Also, we assumed the gas-phase partial pressure of the volatile material was 1.3×10^{-4} dynes cm^{-2} while its saturation vapor pressure was 7.5×10^{-6} dyn cm^{-2} (e.g., Experiment 23 A of Stern et al., 1989). Finally, we assumed a modified diffusion coefficient (D^{eff}-Eq. 2) of 0.1 cm^2 s^{-1}, a surface tension of 30 dyn cm^{-1}, a temperature of 298.15 K, and a radiative heating rate (Q_{rad}) equal to zero.

To obtain the integrated numerical solution, we solved Eqs. 12–15, written as

$$\frac{dC_k}{dt} = \frac{1}{2}\sum_{j=1}^{k}\left(\sum_{i=1}^{k}\frac{\nu_i+\nu_j}{\nu_k}f_{i,j,k}\,\beta_{i,j}C_iC_j\right) - C_k\sum_{j=1}^{N_B}\beta_{i,j}C_j, \quad (12)$$

$$\frac{dC_{V_1k}}{dt} = \sum_{j=1}^{k}\left(\sum_{i=1}^{k}f_{i,j,k}\,\beta_{I,j}C_{V_1i}C_j\right) - C_{V_1k}\sum_{j=1}^{N_B}\beta_{i,j}C_j, \quad (13)$$

$$\frac{dC_{V_2k}}{dt} = \sum_{j=1}^{k}\left(\sum_{i=1}^{k}f_{i,j,k}\,\beta_{i,j}C_{V_2i}C_j\right) - C_{V_2k}\sum_{j=1}^{N_B}\beta_{i,j}C_j + \left(\frac{dC_{V_2k}}{dt}\right)_{growth}, \quad (14)$$

$$\frac{dG}{dt} = -\left(\frac{\rho_{V_2}}{M_{V_2}}\right)\sum_{i=1}^{N_B}\left(\frac{dC_{V_2k}}{dt}\right)_{growth}, \quad (15)$$

simultaneously with SMVGEAR. Equation 12 describes the evolution of number concentration (No. cm^{-3}) of particles in each size bin, $k = 1$ to N_B, due to coagulation only. Equation 13 describes the evolution of volume concentration (cm^3 cm^{-3}) of involatile material (V_1), due to coagulation only. Equation 14 describes the change in volume concentration of volatile material (V_2) due to coagulation, condensational growth, and evaporation. Finally, Eq. 15 describes the change in concentration of the condensing gas

(moles cm^{-3}) due to growth and evaporation. Equation 7 shows the growth derivative referred to in Eqs. 14 and 15.

In the equations, $\beta_{i,j}$ is the rate at which particles of size i coagulate with particles of size j. Also, $f_{i,j,k}$ is the volume fraction of new particles $i+j$ that we partition into bin k. Many values for f are zero; thus, all calculations involving a zero-value for f were eliminated. Jacobson et al. (1994a) show the formulas for $\beta_{i,j}$ and the values for f.

While Jacobson et al. (ibid.) discuss the fully implicit coagulation equations for a monomer size distribution and the semi-implicit equations for a random size distribution, Equations 12–14 describe the fully implicit equations for a random size distribution. An advantage of these new equations is that we can solve coagulation over an entire size distribution with fully implicit equations but with far fewer size bins than the monomer distribution requires. However, the matrix of partial derivatives for coagulation is full; thus, we cannot take advantage of sparse-matrix computer speed increases like we can with other processes such as chemistry and condensational growth.

For the integrated numerical solutions, we solved Eqs. 12–15 over one-half hour time intervals, using variable time steps predicted by SMVGEAR. On the other hand, for model solutions, we time-split coagulation from condensational growth and took three 600-s time intervals for each. For coagulation, the time step equaled the time interval of 600 s. For growth, the time step varied within SMVGEAR. For model solutions to coagulation, we used the semi-implicit method, discussed previously.

For model solutions to growth, we solved Eqs. 7 and 8 simultaneously with SMVGEAR. However, model solutions found with SMVGEAR were different from integrated solutions in one important respect. When time-splitting growth from coagulation, the only variables that we assumed changed during a time step of growth were the gas-phase concentration and aerosol volume of the condensing component. On the other hand, when solving growth and coagulation simultaneously with SMVGEAR, we assumed that the number of particles and the volume of involatile material in each bin changed along with those two parameters. Thus, the matrix of partial derivatives for the fully-integrated solution was much more complex than the matrix for the time-split integrated solution. The advantage of a time-split growth solution is large with respect to computer speed since the matrix of growth partial derivatives is sparse. On the other hand, since the matrix of coagulation partial derivatives in the fully-integrated case is already full, we cannot take advantage of sparse-matrix reductions when we add growth partial derivatives to it.

In sum, the fully-integrated solution is more accurate than the model solution because it solves Eqs. 12–15 exactly under the conditions provided. However, we desired to test how well a time-split solution that included a combination of semi-implicit and fully-implicit techniques compared with the fully integrated result. Figures 3a and 3b show two of the comparisons. For Figure 3a, we ignored the Kelvin effect while for Figure 3b, we did not. The figures show that the model solutions for both whole-particle volume and volatile-component volume matched the integrated solutions at all sizes.

In the case of Figure 3a, the gas-phase partial pressure decreased to the saturation vapor pressure before the end of one-half hour; thus, growth ceased. In the case of Figure 3b, the partial pressure decreased to an effective saturation vapor pressure. Since the Kelvin effect modifies the saturation vapor pressure differently for different-sized particles, vapor continuously transferred between the gas and

aerosol phases. However, after one-half hour, the saturation vapor pressure reached a point where particles above about 0.02 μm were growing from Kelvin-effect transfer and those below had evaporated down to their original cores. Finally, these model solutions required about fifteen times less computer time than did the fully integrated solutions.

In the third set of tests, we compared model growth to an analytical solution shown in Seinfeld (1986). For this solution, particles are uniformly composed and initially distributed lognormally. The analytical number concentration (# cm^{-3}) in each bin i, resulting from the growth of the initial distribution, is

$$C_{i,a}^{t+1} = \frac{C_{T0}}{\sqrt{2\pi}\ln\sigma_g}\frac{d_i dd_i}{\left(d_i^2 - 2A_D t_f\right)} \times \exp\left[-\frac{\ln^2\left(\left(d_i^2 - 2A_D t_f\right)^{1/2}/d_{gno}\right)}{2\ln^2\sigma_g}\right], \tag{16}$$

where d_{gno} is the initial geometric mean number diameter (cm) of the distribution, σ_g is the geometric standard deviation, A_D is a constant growth term ($cm^2\ s^{-1}$) dependent on the diffusion coefficient, saturation ratio, and saturation vapor pressure, d_i is the mean particle diameter (cm) of each discrete bin i, and

$$dd_i = d_i 2^{1/3}\frac{V_{\mathrm{RAT}}^{1/3} - 1}{\left(V_{\mathrm{RAT}} + 1\right)^{1/3}} \tag{17}$$

is the width of discrete bin i for the initial bin structure.

In order to compare moving bin growth solutions to analytical solutions, we fixed the growth rate of each moving bin as

$$C_{vi,m}^{t+1} = C_{vi,m}^{t} + C_i^t \pi r_i A_D\,\Delta t, \tag{18}$$

which is similar to Eq. 11. As with Eq. 11, we grew each bin for several time steps during a time interval and updated the

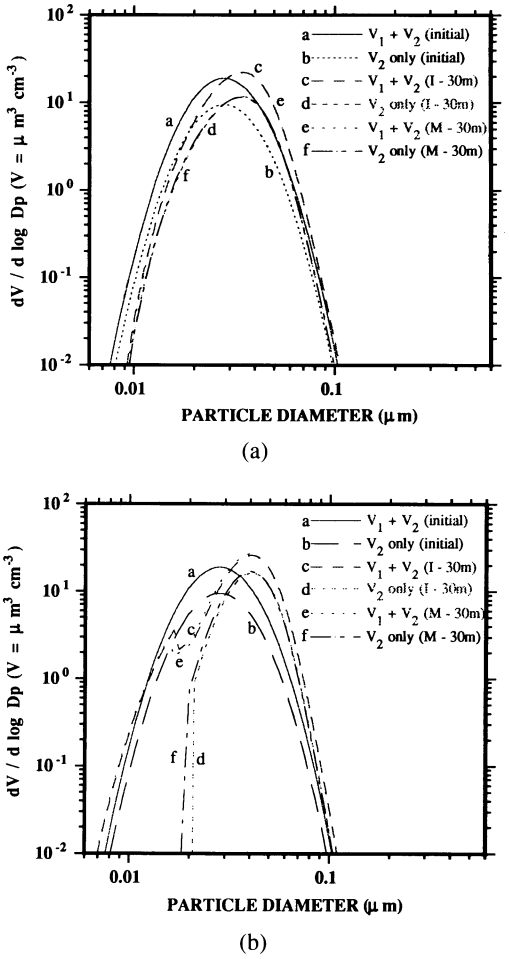

FIGURE 3. Comparisons of model (M) to integrated (I) solutions for the processes of coagulation combined with growth. The particles simulated here contained two components—an involatile core (V_1) and a volatile shell (V_2). Thus, $V_1 + V_2$ identifies the total particle. Equations 7 and 8 describe the growth equations used for both figures. However, the difference between Figs. 3a and 3b are that 3a ignores the Kelvin effect while 3b includes it. To obtain the integrated solutions, we used SMVGEAR to solve Eqs. 12–15, simultaneously, over a continuous time interval. To obtain the model solution, we time-split the semi-implicit coagulation solution from the fully implicit growth solution. The time interval for both analytical and model solutions was $\frac{1}{2}$ h while the time step for splitting model processes was 600 s. The text describes additional conditions for these simulations.

TABLE 1. Initial Distributions and Final Volumes of Three Model Comparisons to Analytical Solutions.

	d_{gno}[a] μm	σ_g[b] —	C_{To}[c] # cm^{-3}	V_{To}[d] μm^3 cm^{-3}	V_{Taf}[e] μm^3 cm^{-3}	V_{Tmf}[f] μm^3 cm^{-3}	V_{RAT}[g] —	Δt[h] s	t_f[i] s
Figure 4	0.2	1.4000	2.260×10^7	1.57×10^5	2.45×10^5	2.46×10^5	1.5	1000.	10,000
Figure 5	0.1	1.1447	8.796×10^6	5.00×10^3	7.06×10^4	7.05×10^4	1.2	0.01	5
Figure 6	0.6	1.3084	6.387×10^6	1.00×10^6	1.34×10^6	1.34×10^6	1.5	100.	10,000

[a]Mean geometric number diameter of the initial lognormal distribution.
[b]Geometric standard deviation of the distribution.
[c]Initial aggregated number concentration.
[d]Initial aggregated volume.
[e]Final aggregated volume from the analytical solution.
[f]Final aggregated volume from the model solution.
[g]Volume ratio of adjacent size bins, used for initializing.
[h]Model time step.
[i]Total time interval for the simulation.

radius and number concentration before each model time step. Table 1 lists initial parameter values, time steps, and time intervals for three model comparisons to analytical solutions. It also shows the final aggregated particle volumes from the analytical and model solutions.

Figure 4 shows the first comparison of analytical to model growth. The initial distribution parameters and the growth rate were from Seinfeld (1986), p. 421. Figure 4 shows that the moving bin solution slightly underpredicted the lower radius bound of the final number concentration.

Figure 5a shows analytical versus model growth and Figure 5b shows model coagulation alone and model coagulation combined with growth. First, the initial distribution and growth rate for these simulations were similar to those presented in Figure 1 of Tsang and Rao (1988). Because the growth rate was fast, we reduced the model time step significantly and increased the number of bins per decade in the initial distribution to 39 (by decreasing V_{RAT} to 1.2). Figure 5a shows that, after five seconds, the moving bin solution paralleled the analytical solution. However, it slightly underpredicted the lower radial end of the analytical distribution.

Figure 5b, shows coagulation alone and coagulation combined with growth. We did not compare these model solutions to analytical solutions. However, elsewhere in this paper and in Jacobson et al. (1994a), coagulation alone was compared to analytical solutions. The results here indicate that, under the conditions presented, both growth and coagulation pushed particles toward larger sizes. How-

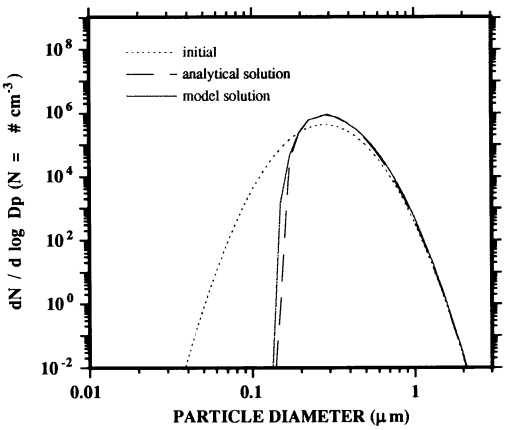

FIGURE 4. Model versus analytical growth solutions. Table 1 lists the initial conditions, some parameter values, and final volume for this simulation. The constant growth term used was $A_d = 1.06 \times 10^{-14}$ cm^2 s^{-1}. To obtain the moving bin solution, we used Eq. 18, and to obtain the analytical solution, we used Eq. 16.

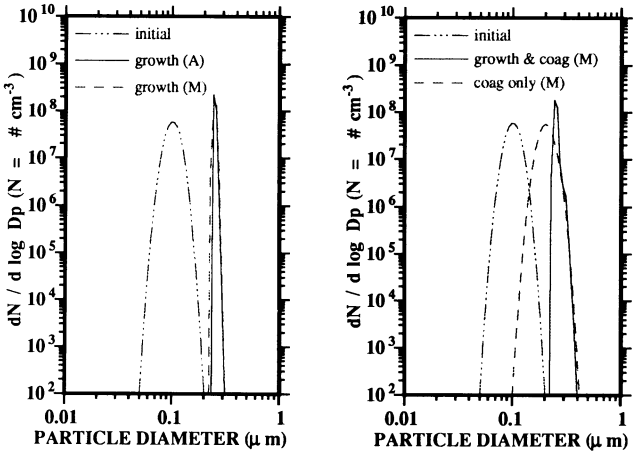

FIGURE 5. Figure 5a shows a comparison of a model (M) to an analytical (A) growth solution. Figure 5b shows model simulations of coagulation only and coagulation combined with condensational growth. Table 1 lists the initial conditions, some parameter values, and final volumes for the comparison of analytical to moving bin growth. The constant growth term used here was $A_d = 1.0 \times 10^{-10}$ cm^2 s^{-1}. To obtain the moving bin solution, we solved Eq. 18, and to obtain the analytical solution, we solved Eq. 16.

ever, while coagulation widened the size distribution, growth narrowed it. Growth combined with coagulation also narrowed the distribution but pushed the leading edge of the distribution further than did growth alone.

Figure 6 shows plots of simulations similar to those in Figure 5, except the initial conditions and growth rate in the new plots are like those used in Figure 2 of Tsang and Rao (1988). The growth rate in this example is much slower than that in the previous example. Again, the moving bin results paralleled those of the analytical solution. Only at the lower radial end of the distribution did the moving bin solution slightly underpredict the analytical distribution. For this example, we initialized the distribution with 18 size bins per decade ($V_{RAT} = 1.5$) and used a model time step of 100 s.

Results shown in Figure 6 indicate that coagulation was more significant than growth under the conditions provided. The fact that coagulation alone and coagulation combined with growth gave solutions similar to each other supports this position. Also, because the initial number concentration was high, we expected coagulation to be important. Finally, because the growth rate was relatively slow (com-

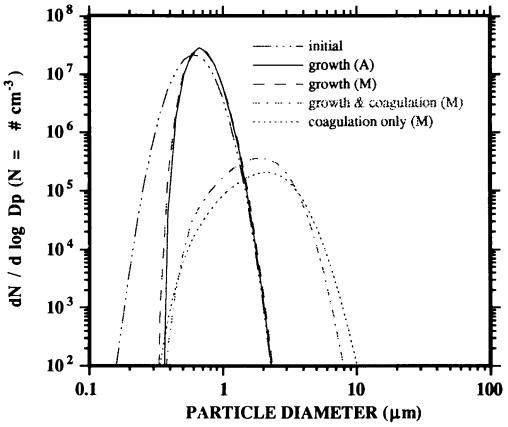

FIGURE 6. This graph shows (a) an initial lognormal aerosol distribution, (b) a comparison of a model (M) to an analytical (A) growth solution, (c) a model simulation of coagulation only, and (d) a model simulation of coagulation combined with condensational growth. Table 1 lists the initial conditions, some parameter values, and final volumes for these simulations. The constant growth term used here was $A_d = 1.0 \times 10^{-13}$ cm^2 s^{-1}. To obtain the moving bin solution, we solved Eq. 18, and to obtain the analytical solution, we solved Eq. 16.

pared with in the previous example) we expected growth to be less important than in the previous example.

V. APPLICATIONS

Here, we demonstrate advantages of using a hybrid grid to simulate growth. Figure 7 shows growth and evaporation of particles containing two components. The initial lognormal distribution of particles consisted of only elemental carbon. We allowed *m*-xylene to condense onto the particles and assumed the same constant pressure difference as in Experiment 23A of Stern et al. (1989). After 6000 s, we removed all gas and allowed the particles to evaporate. To simulate each time step of evaporation, we solved Eqs. 7 and 8 simultaneously. When evaporation occurred, the gas-phase concentration quickly increased to its saturation vapor pressure. To allow evaporation to continue after saturation, we removed all gas at the end of each 100-s time step. Eventually, all condensed aerosol evaporated. Growth occurred much faster than evaporation because we allowed an endless supply of gas to condense over a low vapor pressure. When evaporation occurred, the partial pressure quickly increased to the saturation pressure, inhibiting evaporation. To allow evaporation to continue, we removed gas at the end of a time step.

The purpose of this exercise was not to demonstrate a real situation, but to show the ability of multicomponent particles to grow and then to evaporate back to their original cores. Achieving the original cores is difficult with fixed-bin growth methods, but is straightforward with a moving bin method.

Figure 8 stresses a point similar to that made in Figure 7. However, in the new case, we show results from 12 cycles of growth and evaporation of a fog. In this simulation, we started with a trimodal lognormal distribution of elemental carbon.

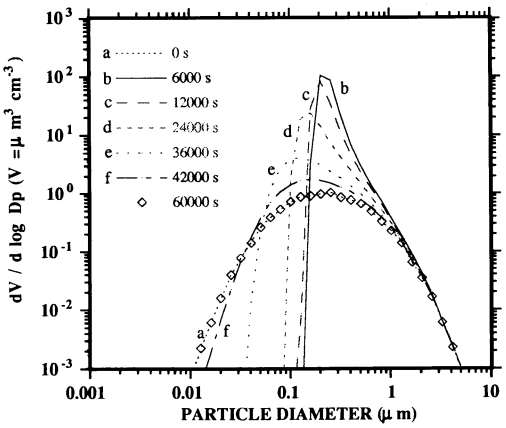

FIGURE 7. Model simulation of condensational growth followed by evaporation. The initial aerosol consisted of a lognormal distribution of elemental carbon only, with $d_{gno} = 0.129$ μm and $\sigma_g = 2.00$. Subsequently, *m*-xylene grew for 6000 s. At 6000 s, we set the gas-phase partial pressure to zero and allowed evaporation to occur. To speed evaporation, we removed all existing gas every 100 s. This figure shows that particles simulated with moving bins evaporated back to their original cores.

By alternating the temperature every 600 s, we changed the relative humidity, allowing a fog to repeatedly grow and evaporate. For each growth, the fog achieved the same distribution as for the previous growth, and for each evaporation, the fog shrunk to its initial core distribution. Achieving the initial core distribution with a stationary bin method is more difficult than with a hybrid or moving bin method. Figure 8 also shows that the Kelvin effect prevented some particles from growing to fog-size drops. To obtain the results for Figure 8, we solved Eqs. 7 and 8 with SMVGEAR over a hybrid size grid.

Next, Figure 9 shows a 4-h model comparison of fog growth alone to fog growth coupled with coagulation. The initial distribution was the same as in Figure 8, the initial humidity was about 100.5%, and the temperature was constant at 287.5 K.

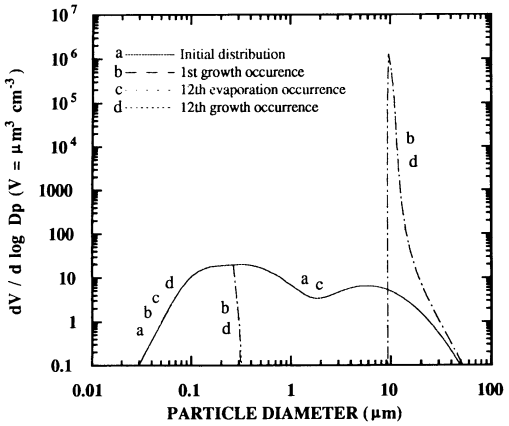

FIGURE 8. Model results of 12 cycles of growth and evaporation. The initial distribution of elemental carbon was trimodal and the initial temperature and relative humidity were 290 K and 85.9%, respectively. After 600 s, the temperature decreased to 287.5 K, causing the relative humidity to increase to 100.5% and water to condense rapidly onto the core material to form a fog. The figure shows the volume distribution of the total particle (elemental carbon plus water). Because the saturation vapor pressure of particles below about 0.3 μm exceeded the actual vapor pressure multiplied by the Kelvin effect, these particles did not grow. After another 600 s we increased the temperature again to 290 K, causing the relative humidity to fall back to 85.9% and particles to evaporate to their original core sizes. We repeated this growth-evaporation cycle a total of 12 times. The figure demonstrates that allowing particles with the same core sizes to grow and evaporate independently of particles with different core sizes preserves the initial core distribution and permits continuous duplication of fog growth.

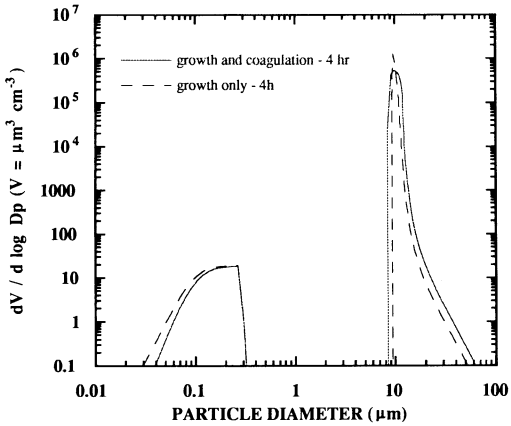

FIGURE 9. A four-hour model comparison of fog growth alone compared to fog growth coupled with coagulation. The initial distribution was the same as that in Figure 8, the initial humidity was about 100.5%, and the temperature stayed constant at 287.5 K throughout the simulation. The figure shows the volume distribution of the total particle (carbon plus water) at the end of the simulation. The text describes remaining conditions.

In both cases, each of the 24 time-intervals was 10 min. We solved coagulation with the semi-implicit method, using time steps equal to the time interval (no iteration required). The coagulation kernel included the effects of Brownian motion, convective diffusion enhancement, gravitation, turbulent shear, and turbulent inertial motion (Fuchs, 1964; Pruppacher and Klett, 1978; Saffman and Turner, 1956). Also, in both cases, we solved growth with SMVGEAR, which uses variable time steps.

Figure 9 shows that coagulation slightly broadened the cloud-drop portion of the distribution and moved unnucleated cores to slightly larger sizes. While Brownian coagulation affected particles primarily less than 1 μm in diameter, differential fall velocities and turbulent motions were responsible for most coagulation in particles larger than 1 μm. Finally, while most growth occurred within the first few minutes of the simulation, coagulation continued to affect all modes of the distribution during the entire simulation period.

Figures 10a and 10b show condensational growth of sulfuric acid and water and the corresponding conservation of the gas phase during growth. The initial distri-

bution of elemental carbon was the same as in Figure 8. Also, the initial gas concentration of sulfuric acid was 10^{11} cm^{-3}, the ambient temperature was 287.5 K, and the relative humidity was 81%. At this temperature and humidity, the saturation number density of sulfuric acid over a flat surface is about 10^{1} cm^{-3}. The difference in ambient versus saturation densities forced gas-phase sulfuric acid to condense.

When sulfuric acid condenses, water condenses simultaneously. As the acid dissociates into ions, each ion attracts liquid water molecules. A convenient technique to estimate the amount of water that condenses to satisfy the change in ion content of the aerosol is the ZSR methods (Zdanovskii, 1948; Stokes and Robinson, 1966; Cohen et al., 1987; Pilinis and Seinfeld, 1987b). We used the ZSR method combined with an equilibrium model (Jacobson et al., 1994b) to calculate both the amount of water that condensed with sulfuric acid and the distribution of HSO_4^-, SO_4^{2-}, and H^+ ions that resulted from the condensation of acid.

In sum, the processes included to obtain Figures 10a and 10b were condensational growth (gas and aerosol phase solved simultaneously with SMVGEAR) and chemical equilibrium (including calculation of aerosol water content). Figure 10a shows the growth of the aerosol distribution. The final distribution contained about 45.3 $\mu g\ m^{-3}$ of liquid water, compared with 10.7 $\mu g\ m^{-3}$ of HSO_4^-, 5.4 $\mu g\ m^{-3}$ of SO_4^{2-}, and 0.1 $\mu g\ m^{-3}$ of $H_2SO_4(aq)$. Thus, about 74% of the increase in aerosol mass was due to water condensation although sulfuric acid was the initial condensing species.

Figure 10a also shows that the resulting aerosol distribution peaked near 0.65 μm diameter. While this distribution did not account for gas-phase chemistry, emissions, deposition, transport, and other processes, the resulting diameter fell within the accumulation mode. Hering and Friedlander (1982) measured ambient sulfur distributions and found an average mass median diameter of about 0.54 μm when the maximum humidity ranged from 69%–100%.

Finally, Figure 10b shows the reduction in gas-phase sulfuric acid during the pe-

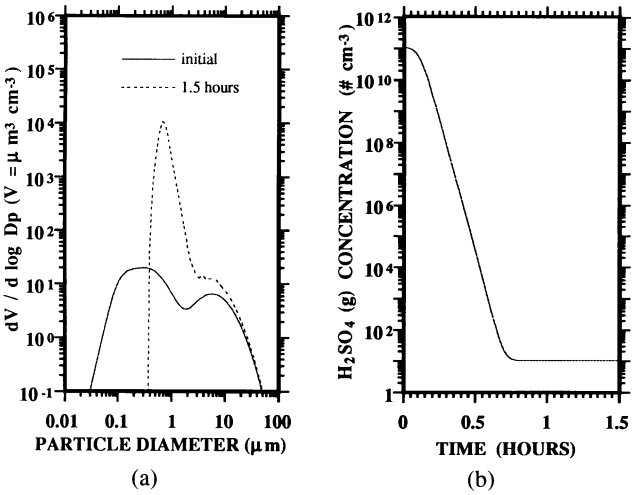

FIGURE 10. Model simulation of condensational growth of sulfuric acid and water onto a trimodal, lognormal elemental carbon initial distribution. Figures 10a shows the growth of the particle and 10b shows the corresponding depletion in gas-phase sulfuric acid to its saturation number density. As sulfuric acid condensed, it attracted water. In fact, about 74% of the mass added to the distribution was liquid water. Within the sulfuric acid–water mixture, hydrogen ions, sulfate, and bisulfate ions existed in equilibrium.

riod of condensation. Figure 10b shows that condensation actually ceased after about 45 min of simulation.

VI. CONCLUSIONS

We discussed an aerosol model that uses a hybrid size grid that has characteristics of both a stationary and moving grid. For the most part, the core volume of particles in each size bin remains fixed while the volatile volume of particles fluctuates. Allowing particles of one core volume to grow and evaporate independently of particles of other core volumes eliminates numerical diffusion. Furthermore, it permits grown particles to condense back to their exact core sizes and particles of the same size to have different composition.

For this model, we set up and solved growth equations that conserve mass between the gas and size-resolved aerosol phases. To calculate the solution to the growth equations, we used SMVGEAR, a sparse-matrix vectorized Gear-type code. SMVGEAR exploits the sparsity of the matrix of partial derivatives to solve the growth equations. Furthermore, it vectorizes around the grid-cell dimension, allowing relatively rapid solutions to first-order ordinary differential equations in large grid domains.

Next, we modified the coagulation code of Jacobson et al. (1994a) to permit coagulation over the hybrid grid structure. The modified code allows us to partition each coagulated particle and its total volume between particles of two size bins—one with particles of smaller core volume and the other with particles of larger core volume than that of the coagulated particle.

To test growth and coagulation over the hybrid grid structure, we compared results to analytical and integrated numerical solutions. For the integrated solutions, we devised fully implicit coagulation and growth equations and solved them with SMVGEAR. When computer speeds increase further, fully integrated solutions will become more feasible over large grid domains. However, for now, the time-split model scheme presented here predicts solutions similar to those of the integrated solutions while taking much less computer time.

We thank the Environmental Protection Agency for partial support under grant CR-812771-03-0 and the National Science Foundation for partial support under grant A7M-89-11836. We also thank NAS computer center at NASA Ames Research Center, Mountain View, California for permitting our use of a CRAY 90 computer.

REFERENCES

Barkstrom, B. R. (1978). *J. Atmos. Sci.* 35:665–673.

Bassett, M., Gelbard, F., and Seinfeld, J. H. (1981). *Atmos. Environ.* 15:2395.

Beard, K. V., and Pruppacher, H. R. (1971). *J. Atmos. Sci.* 28:1455–1464.

Brock, J. R., Zehavi, D., and Kuhn, P. (1986). *J. Aerosol Sci.* 17:11–22.

Brock, J. R., and Oates, J. (1987). *J. Aerosol Sci.* 18:59–64.

Cohen, M. D., Flagan, R. C., and Seinfeld, J. H. (1987). *J. Phys. Chem.* 91:4575–4582.

Friedlander, S. K. (1983). *Ann. NY Acad. Sci.* 404:354–364.

Frossling, N. (1938). *Beitr. Geophys.* 52:170.

Fuchs, N. A. (1964). *The Mechanics of Aerosols.* (R. E. Daisley and M. Fuchs, Translation) Pergamon Press, New York.

Fuchs, N. A., and Sutugin, A. G. (1971). Highly dispersed aerosols, in *Topics in Current Aerosol Research* (G. M. Hidy and J. R. Brock, ed.). Pergamon Press, New York, Vol. 2, pp. 1–60.

Gelbard, F., and Seinfeld, J. H. (1978). *J. Comp. Phys.* 28:357.

Gelbard, F., and Seinfeld, J. H. (1980). *J. Colloid Interface Sci.* 78:485–501.

Gelbard, F. (1990). *Aerosol Sci. Technol.* 12:399–412.

Hering, S. V., and Friedlander, S. K. (1982). *Atmos. Environ.* 16:2647–2656.

Jacobson, M. Z., and Turco, R. P. (1994). *Atmos. Environ.* 28A:273–384.

Jacobson, M. Z., Turco, R. P., Jensen, E. J., and Toon, O. B. (1994a). *Atmos. Environ., Part A.*, 28A: 1327–1338.

Jacobson, M. Z., Turco, R. P., and Tabazadeh, A. (1994b). *J. Geophys. Res.*, in review.

Keith, C. H., and Arons, A. B. (1954). *J. Met.* 11:173–184.

Kim, Y. P., and Seinfeld, J. H. (1990a). In *Proceedings of the 3rd International Aerosol Conference, Science, Industry, Health and Environment*, Pergamon Press, Oxford, pp. 138–141.

Kim, Y. P., and Seinfeld, J. H. (1990b). *J. Colloid Interface Sci.* 135:185–199.

Langmuir, I. (1944). *Super cooled Droplets in Rising of Cold Saturated Air*. General Electric Company, Schenectady, N.Y. 150 pp.

Lee, K. W. (1985). *J. Colloid and Interface Sci.* 108:199–206.

Middleton, P., and Brock, J. R. (1976). *J. Colloid Interface Sci.* 54:249–264.

Mordy, W. (1959). *Tellus* 11:16–44.

Neiburger, M., and Chien, C. W. (1960). In *Physics of Precipitation, Proceedings of the Cloud Physics Conference, Woods Hole, Massachusetts, June 3–5, 1959*. AGU, pp. 191–210.

Pilinis, C., Seinfeld, J. H. and Seigneur, C. (1987a). *Atmos. Environ.* 21:943–955.

Pilinis, C., and Seinfeld, J. H. (1987b). *Atmos. Environ.* 21:2453–2466.

Pruppacher, H. R., and Klett, J. D. (1978). *Microphysics of Clouds and Precipitation.* Reidel, The Netherlands.

Rao, N. P., and McMurry, P. H. (1989). *Aerosol Sci. Technol.* 11:120–133.

Rooth, C. (1957). *Tellus* 9:372–377.

Saffman, P. G., and Turner, J. S. (1956). *J. Fluid Mech.* 1, 16–30.

Seigneur, C. (1982). *Atmos. Environ.* 16:2207–2228.

Seinfeld, J. H. (1986). *Atmospheric Chemistry and Physics of Air Pollution.* John Wiley, New York.

Smolarkiewicz, P. K. (1983). *Mon. Weather Rev.* 111:479–486.

Stern, J. E., Flagan, R. C., and Seinfeld, J. H. (1989). *Aerosol Sci. Technol.* 10:515–534.

Stokes, R. H., and Robinson, R. A. (1966). *J. Phys. Chem.* 70:2126–2130.

Toon, O. B., Turco, R. P., Westphal, D., Malone, R., and Liu, M. S. (1988). *J. Atmos. Sci.* 45:2123–2143.

Toon, O. B., Turco, R. P., Jordan, J., Goodman, J., and Ferry, G. (1989). *J. Geophys. Res.* 94:11,359–11,380.

Tsang, T. H., and Brock, J. R. (1983). *Aerosol Sci. Technol.* 2:311–320.

Tsang, T. H., and Brock, J. R. (1986). *Aerosol Sci. Technol.* 5:385–388.

Tsang, T. H., and Hippe, J. M. (1988). *Aerosol Sci. Technol.* 8:265–278.

Tsang, T. H., and Huang, L. K. (1990). *Aerosol Sci. Technol.* 12:578–597.

Tsang, T. H., and Korgaonkar, N. (1987). *Aerosol Sci. Technol.* 7:317–328.

Tsang, T. H., and Rao, A. (1988). *Aerosol Sci. Technol.* 9:271–277.

Turco, R. P., Hamill, P., Toon, O. B., Whitten, R. C., and Kiang, C. S. (1979a). *J. Atmos. Sci.* 36:699–717.

Turco, R. P., Hamill, P., Toon, O. B., Whitten, R. C., and Kiang, C. S. (1979b). *NASA Tech. Publ.* (TP) 1362, iii-94.

Varoglu, E., and Finn, W. D. L. (1980). *J. Comp. Phys.* 34:371–389.

Warren, D. R., and Seinfeld, J. H. (1985). *Aerosol Sci. Technol.* 4:31–43.

Whitby, E. R. (1985). *The Model Aerosol Dynamics Model. Part I.* Report to the U.S. Environmental Protection Agency, Dept. of Mechanical Engineering, University of Minnesota, Minneapolis.

Wu, J. J., and Flagan, R. C. (1988). *J. Colloid Interface Sci.* 123:339.

Zdanovskii, A. B. (1948). *Zhur. Fiz. Khim.* 22:1475–1485.

Received November 11, 1993; revised June 14, 1994.